Towards a Better Mechanistic Understanding of the Degradation Processes of Perovskite Solar Cells

Carlos Biaou

Electrical Engineering and Computer Sciences
University of California at Berkeley

Technical Report No. UCB/EECS-2018-3
http://www2.eecs.berkeley.edu/Pubs/TechRpts/2018/EECS-2018-3.html

January 23, 2018

Acknowledgement

This work was made possible by a National Science Foundation Graduate Research Fellowship, a Chancellor's Fellowship, and a Jack Kent Cooke Foundation Graduate Scholarship. Prof. Ana Arias' gracefulness and generosity is applauded for sharing her lab tools, which were critical in carrying out this study to completion. Thanks also go to my collaborators Matthew McPhail and Lance Go for their considerable support. Jeremy Smith, William Scheideler, and Gerd Grau are also hereby recognized for the insightful conversations.

Towards a Better Mechanistic Understanding of the Degradation Processes of Perovskite Solar Cells

by Carlos Koladélé Biaou

Research Project

Submitted to the Department of Electrical Engineering and Computer Sciences, University of California at Berkeley, in partial satisfaction of the requirements for the degree of **Master of Science, Plan II**.

Approval for the Report and Comprehensive Examination:

Committee:

Professor Vivek Subramanian
Research Advisor

Thursday, January 11, 2018

(Date)

* * * * * * *

Professor Ana Claudia Arias
Second Reader

Tuesday, January 23, 2018

(Date)

Abstract:

In 2009, a group in Japan introduced a perovskite solar cell delivering 3.8% efficiency [1]. Then in 2012, Henry Snaith's group demonstrated a solution-processed perovskite solar cell with an efficiency of 10.9% [2]. Ever since, perovskite based solar devices have soared to the top of the scene in photovoltaic research with a maximum confirmed efficiency of 22.1% [3]. Though progress has been extremely fast, perovskites will remain at the forefront of photovoltaic research because of the great number of mysteries that have yet to be solved. One of those is the ongoing struggle of the perovskite solar cells' stability in atmospheric conditions.

There have been numerous theoretical and experimental studies of certain perovskites' degradation pathways. These usually involve theorizing about the effects of humidity and oxygen on the active layer or illuminating the cell under no load and tracking its power conversion efficiency. However, the term perovskite merely refers to a structure. Thus, there is an entire class of materials that exhibit photovoltaic behavior for the purpose of providing power to an electrical load. To fill this gap in knowledge, we studied two types of perovskite—cesium formamidinium lead triiodide ($Cs_{0.2}(CH(NH_2)_2)_{0.8}PbI_3$ or $Cs_{0.2}FA_{0.8}PbI_3$) and methylammonium lead triiodide ($CH_3NH_3PbI_3$ or $MAPbI_3$)—and tracked their crystallographic, optical, and electrical characteristics under various load, humidity, and temperature conditions. These studies give us experimental insight into the degradation process that occurs in these systems. Such studies thus form an excellent starting point for understanding the degradation phenomena that affect such devices and have important implications for their future viability.

Table of Contents

Introduction:

Silicon based solar cells have dominated the current solar energy market for many decades. Indeed, they are inexpensive, reliable, and certified for a lifetime of beyond 25 years [4]. However, silicon is not an ideal photovoltaic material because of its indirect band gap. Furthermore, the efficiency of a single junction silicon solar cell has plateaued around 25% since 2000 [3], indicating that we have reached a technological limit. To further reduce the cost of commercially available solar cells, there are two main avenues to explore: (1) increasing the power conversion efficiency (PCE) of the solar cell and (2) reducing the manufacturing cost of the cell. Using a multi-junction cell, it is possible to increase the efficiency of the cell (up to 46% as of 2017 [3]). Increasing the PCE while maintaining the manufacturing cost has proven to be more of challenge until the introduction of perovskite solar cells. With their low manufacturing cost, ease of fabrication, and higher absorption than silicon in the blue region of the visible spectrum, perovskite solar cells offer an option as a complement to silicon in a tandem cell to increase the PCE of commercial solar cells, or alternatively, as a standalone low-cost cell technology.

The name perovskite refers to the ABX_3 crystal structure of the absorber material, where, in the case of solar devices, A is usually, but not necessarily, a methylammonium ion, B is a lead ion, and X is a halogen ion (I^-, Br^-, Cl^-). The $CH_3NH_3PbX_3$ structure has band gaps between 2.30eV and 1.57eV depending on the halogen compound used. Perovskites are particularly attractive because of their long free carrier diffusion length (usually above 1μm) and the predominance of free electrons and holes as opposed to excitons [5], thus enabling a seamless charge separation at room temperature. With a relatively low thermal budget, and a potential to achieve ~31% PCE according to detailed balance theory analyses, perovskites present themselves as viable options for forming a high performance solar cells. However, there are two major bottlenecks that temper its use in manufacturing thus far: (1) the relatively fast degradation under atmospheric and high humidity conditions, and (2) the use of the toxic heavy metal lead in its formulation. There have been efforts to substitute lead with tin, which is in the same group-14 as lead on the periodic table. However, Sn^{2+} is unstable in air and prefers the more stable Sn^{4+} form; consequently, tin-based perovskite SCs degrade in matters of seconds in atmospheric conditions. On the other hand, degradation of lead based perovskite is slower but not enough to guarantee usage for more than 25 years.

In this study, we systematically study the effects of electrical load, temperature, perovskite type, and humidity on the electrical performance and the intrinsic properties of the perovskite solar cells. This data set can then form the basis for future studies on stability of this important technology.

Perovskite Degradation Literature Review:

Degradation and stability concerns have always been a major trust within the perovskite research community. Many studies have focused on encapsulation techniques to prevent UV exposure [6], oxygen exposure [7], and moisture penetration [7]. Each of those techniques has provided incremental improvement of the stability of the solar cells, some showing promising stabilities of over a year of operation [8]. However, all of these fall short from the commercially viable goal of 25 years of stable operation, particularly for tandem cell integration with silicon. To tackle this issue, the intrinsic properties and degradation processes of perovskite solar cells must be addressed directly to move from incremental to major advancements in stability. Some studies share that approach but have attacked the issue piecewise.

Indeed, Pearson et al. [9] focused on studying the kinetics and mechanics of oxygen degradation of mesoporous $Al_2O_3/CH_3NH_3PbI_{3-x}Cl_x$ perovskite solar cells. They have observed that the degradation of the cells occurred under operation even in dry conditions resulting in the decomposition of the perovskite itself. Specifically, it was proposed that photogenerated electrons in the perovskite permit a reaction between the methylammonium organic cation and superoxide, a process that results in the decomposition of $CH_3NH_3PbI_3$ with methylamine, PbI_2, I_2, and H_2O as byproducts:

$$CH_3NH_3PbI_3 + O_2^{\bullet -} \xrightarrow{\text{Deprotonation}} CH_3NH_2 + PbI_2 + \frac{1}{2}I_2 + H_2O$$

Transient photocurrent (TPC) and photovoltage (TPV) reveal that the degradation is related to charge build-up in the perovskite layer. Specifically, they argue that photocurrent loss at low cumulative oxygen exposure is due to the formation of charge barriers at the cell's electrode interface layer that act to screen the built-in field. Thereby, the efficiency of charge extraction is reduced following the underlying mechanism of the increase of mobile defects and electronic traps within the active layer. Then, at higher cumulative oxygen exposure, the loss of photocurrent is due to material degradation more severe than just inducing defects leading to decreased light harvesting efficiency and sub-microsecond recombination.

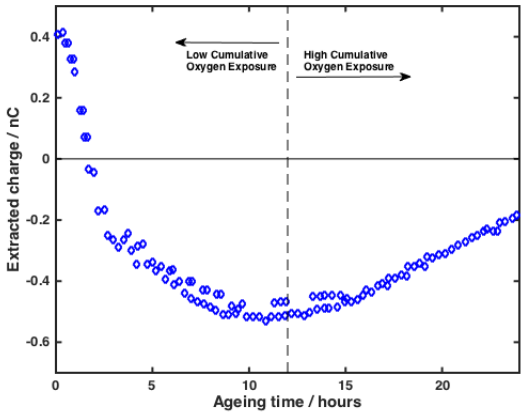

Figure 1: Integrated current during transient decay plotted against ageing time (adapted from [9]).

Connings et al. [10], on their end, have solely focused on the intrinsic thermal instability of methylammonium lead trihalide perovskite. They demonstrate that significant decomposition effects already occur during annealing of methylammonium lead triiodide perovskite at 85ºC even in inert atmosphere. Indeed, even in the absence of oxygen and water, the perovskite is disintegrating, and so are its building blocks. The MAI is decomposing in the same fashion as in the presence of oxygen and water but at a slower rate. Also, they show that, contrary to common belief, not all Pb^{2+} is spent in the form of PbI_2 upon degradation, as evidence by an increased contribution at the Pb^0 energy position with the most plausible explanation being that metallic Pb clusters are formed upon degradation. They claim that these processes lead to an increased series resistance and the creation of interfacial traps since most of the degradation occurs at the surface exposed. The results are lower charge extraction leading to lower efficiencies.

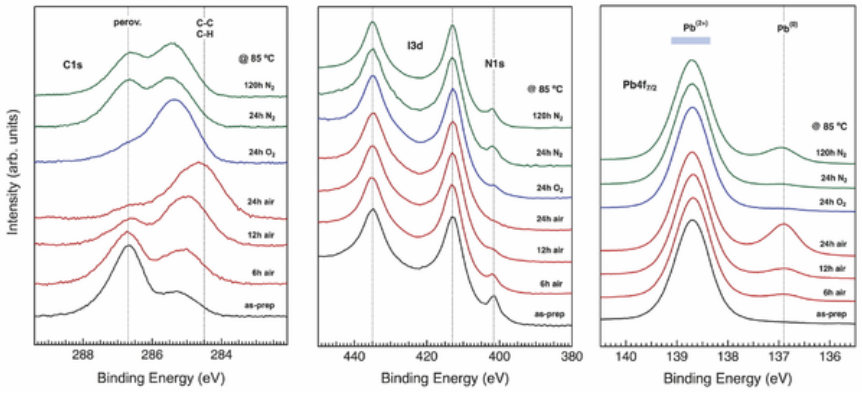

Figure 2: XPS measurements on degraded ITO/TiO_2/perovskite samples that were subjected to 85ºC for 24h in different atmospheres: C1s (left panel), I3d and N1s (middle panel), and $Pb4f_{7/2}$ (right panel) binding energy regions [10].

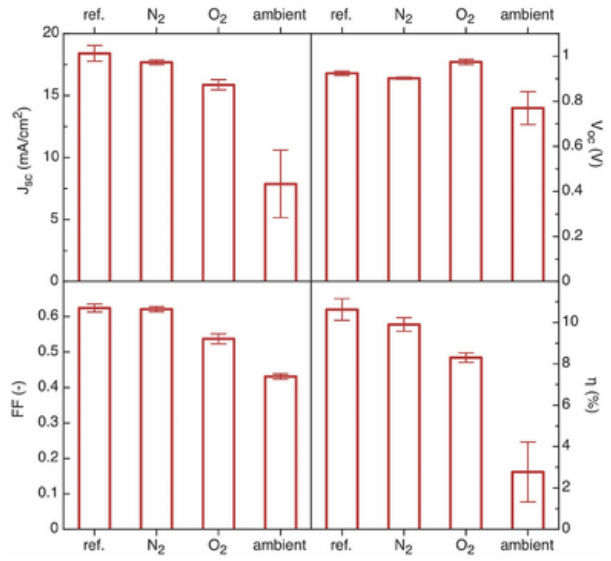

Figure 3: Photovoltaic parameters of solar cells prepared with perovskite layers that were subjected to a temperature of 85°C for 24h in different atmospheric conditions. The error bars reflect the standard deviation of a batch of four solar cells for each atmospheric condition [10].

On their end, Christians et al. [11] have chosen to study humidity's effect on $MAPbI_3$ cells. They show that H_2O exposure does not simply cause $MAPbI_3$ to revert to PbI_2, but it also has the potential of forming a hydrate product similar to $(CH_3NH_3)_4PbI_6 \bullet 2H_2O$ in the dark as shown the XRD spectra. While significant changes are observed in the absorption spectra, the presence of the hydrate has no significant effect on the charge carrier dynamics at short times, which could be rationalized by the fact that defects in the $MAPbI_3$ crystal lattice tend to form only shallow trap states, while trap-mediated recombination mechanisms are essentially absent on the nanosecond time scale [12]–[17]. The IV characteristics, on the other hand, decrease sharply, and they hypothesize that the drop in long-range charge transport is due to weak hydrogen-bonding interaction between the organic cation and the metal halide octahedral and/or the strong hydrogen interaction between the organic cation and H_2O.

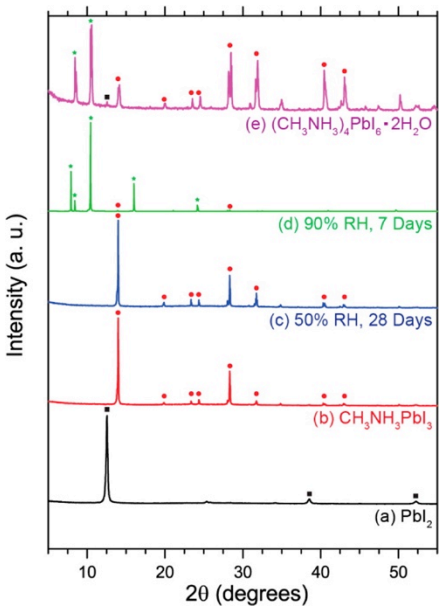

Figure 4: XRD patters of (a) PbI_2, (b) a pristine $MAPbI_3$ film, (c) a $MAPbI_3$ film that has been stored at 50% RH in the dark for 28 days, (d) a $MAPbI_3$ film that has been stored at 90% RH in the dark for 7 days, and (e) $(CH_3NH_3)_4PbI_6 \cdot 2H_2O$ crystals. Characteristic XRD peaks are labeled on the figure for PbI_2 (black square), $MAPbI_3$ (red circle), and the $MAPbI_3$ hydrate (green star) [11].

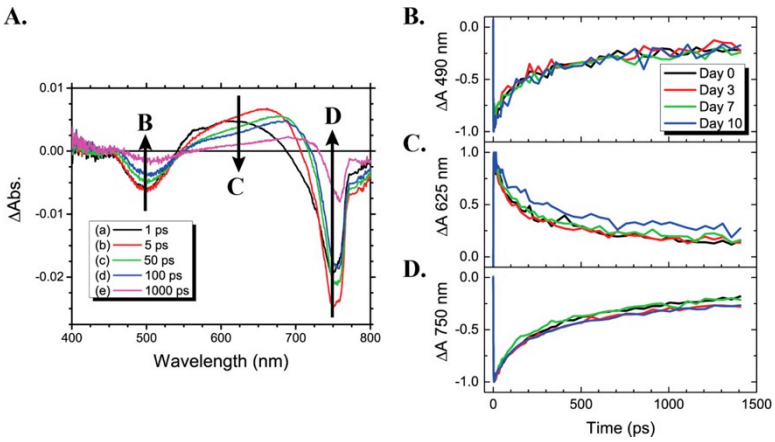

Figure 5: (A) Representative femtosecond transient absorption spectra of the perovskite film showing wavelengths at which the recovery kinetics were probed. Time-resolved kinetic traces assembled at (B) 490 nm, (C), 625 nm, and (D) 760 nm for a perovskite film stored between 0 and 10 days at 90% RH at room temperature in the dark [11].

The only study to our knowledge to have employed a systematic investigation of multiple competing degradation factors is one from Domanski et al. [18]. Indeed, they investigate the competing effects of illumination, atmosphere, humidity, temperature, and electrical load on perovskite solar cells to initiate a discussion on standardization of stability measurements rather than one on mechanistic processes. The investigation focuses on a $Cs_5(FA_{83}MA_{17})_{95}Pb(I_{83}Br_{17})_3$ cell using a mesoporous architecture. The key claim here is that

once the cell is no longer under load, some losses tend to be reversible, and the cell recovers a significant portion of its original power conversion efficiency when left in the dark overnight. They suggest that building a set-up with a controlled environment would limit the observation of unrelated effects outside of the factors under study.

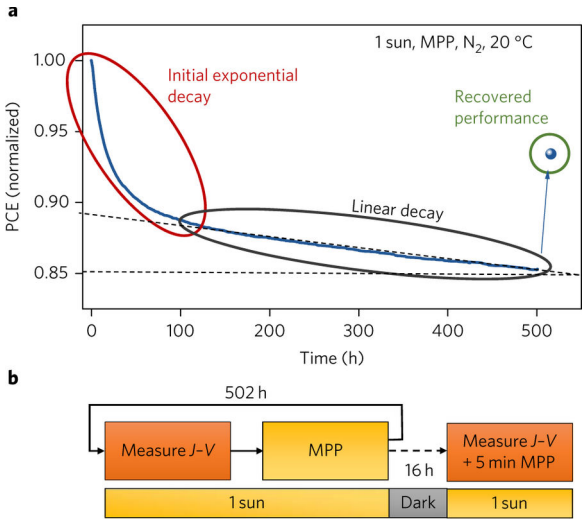

Figure 6: (a) The device shows an initial exponential loss region, followed by a slower linear region. A slope can be fitted to the linear region (broken line) to estimate device lifetime, T_{80}. The device can recover part of its initial performance after being kept in the dark—in this case for 16 hours. The device was aged under a white LED lamp. (b) A schematic of the ageing procedure combining MPP tracking and periodic *J–V* scans. One has to consider the balance between the time spent during *J–V* scans and that at the MPP, as degradation may be different during *J–V* sweeps and at the MPP. For this study, we performed 100 mV s^{-1} scans every 15 min, which results in devices spending 98% of the time at the MPP. However, there is no 'right' balance. More frequent *J–V* scans may sometimes be more suitable to resolve very fast degradation (for example, rapid bleaching). On the other hand, frequent *J–V* scans are not required when the devices appear stable [18].

In sum, the vast majority of studies on the intrinsic nature of the degradation processes in perovskite solar cells have focused on evaluating the effect of a single factor at a time. These studies are invaluable in expanding the knowledge of this unorthodox class of materials. However, if the goal is to create a viable product, more attention needs to be paid towards realistic operating conditions, where second and, perhaps, third order effects may arise from using the solar cell under load and in the elements. Indeed, the community should seek to catalog the behavior of the devices under those conditions, study the impact on various intrinsic properties for different perovskite formulations and different solar cell architectures, and formulate plans to strengthen the inner structure of these devices. The study by Domanski et al. [18], mentioned above, is great for initiating that discussion. In the study herein, effects arising from first and second order interactions of temperature, humidity, perovskite type, and load are additionally

systematically evaluated during degradation. These experiments are building blocks upon which further investigation of the microstructure of the solar cell will potentially lead to major improvements in stability.

Experimental Details:

Sample Preparation

FTO coated glass (7Ω/sq) purchased from MSE supplies were used as substrates for the solar cells. The substrates were successively cleaned in (1) a 2% mixture of Hellmanex (Sigma-Aldrich) in DI water, (2) acetone, and (3) isopropanol for 5min each in a sonicator. They were then exposed for 3 min under oxygen plasma prior to spinning the electron transport layer. The electron transport layer was prepared from (1) a titanium isopropoxide solution purchased from Solaronix to form the compact TiO_2 and (2) a colloidal dispersion of TiO_2 nanoparticles of <50nm also purchased from Solaronix. The hole transport material precursor was prepared from a solution of spiro-OMeTAD (Sigma-Aldrich, 288mg) in chlorobenzene (Sigma-Aldrich, 4mL) and doped with a 520mg/mL solution of bis(trifluoromethane)sulfonimide lithium in acetonitrile (Sigma-Aldrich, 70μL) and 4-tert-Butylphenol (Sigma-Aldrich, 115.2μL).

Perovskite Precursor Preparation

Two different perovskite precursors were prepared for this study. The $Cs_{0.2}FA_{0.8}PbI_3$ precursor was prepared from a solution of CsI (187mg), FAI (495mg), and PbI_2 (1626mg) in a 1:9 ratio of DMF (3.24mL) to DMSO (0.36mL). The solution was then stirred until complete homogeneity. The $MAPbI_3$ precursor was prepared from a solution of CH_3NH_3I (395mg) and PbI_2 (1153mg) in a 1:9 ratio of DMF (2.25mL) to DMSO (0.25mL). The solution was then stirred until complete homogeneity. All reagents were purchased from Sigma-Aldrich.

Solar Cell Fabrication

First, under low humidity conditions, 100μL of the titanium isopropoxide precursor was spun on the FTO substrates at 5000rpm and 2000rpm/s for 30s. They were then dried at 150ºC for 10min of a hotplate followed by sintering under atmospheric conditions at 500ºC for 30min in a furnace to form the TiO_2 blocking layer. After the substrates have cooled down to room temperature and under atmospheric conditions, the colloidal

dispersion of TiO_2 nanoparticles was spun on top of the blocking layer at 5000rpm and 2000rpm/s for 30s. They were then dried at 150ºC for 2min of a hotplate followed by a sintering at 475ºC for 30min in a furnace to form the TiO_2 mesoporous layer. The substrates were moved to an N_2 environment for the deposition of the perovskite layer. The 100μL of perovskite precursor was spun for step 1 at 1000rpm/s and 500rpm/s for 10s and for step 2 at 6000rpm and 3000rpm/s for 25s. At 10s within step 2, droplets of cholorobenzene were deposited at a rate of 1mL/min for a total volume of 100μL. The perovskite was then annealed for 10min at 100ºC on a hotplate to form the perovskite active layer. Once cooled back to room temperature, the solution of spiro-OmeTAD in cholorobenzene was spun on top of the stack at 4000rpm and 2000rpm/s for 30s to form the hole transport material. Finally, 80nm of Au were thermally evaporated to form the contacts. The active area, defined as the overlap between the FTO and Au contacts, is $0.05cm^2$. The fabrication process was adapted from a report by Yi et al. [19].

Measurements and Degradation Set-up

The essence of this study is to understand the degradation of solar performance in settings that reflect as much as possible realistic conditions. Indeed, the temperature bounds chosen reflect room temperature (25ºC) and the highest ever recorded temperature on Earth (55ºC), whereas the humidity levels chosen (30% and 60%) reflect levels typically encountered in the Bay Area. In addition, two perovskite formulations and loading conditions were chosen. Changing all these factors simultaneously allows for the extraction of effects arising from interactions between factors that would be difficult to see otherwise but does reflect how nature works. The various combinations employed are summarized in **Table 1.**

Temperature (ºC)	Perovskite Type	Humidity (%)	Loading (1kΩ)
55	$Cs_{0.2}FA_{0.8}PbI_3$	30	Load
55	$Cs_{0.2}FA_{0.8}PbI_3$	60	Load
25	$MAPbI_3$	30	Load
55	$MAPbI_3$	30	Load
25	$MAPbI_3$	60	Load
25	$Cs_{0.2}FA_{0.8}PbI_3$	30	Load
55	$Cs_{0.2}FA_{0.8}PbI_3$	30	No Load
55	$Cs_{0.2}FA_{0.8}PbI_3$	60	No Load
25	$MAPbI_3$	30	No Load
55	$MAPbI_3$	30	No Load
25	$MAPbI_3$	60	No Load
25	$Cs_{0.2}FA_{0.8}PbI_3$	30	No Load

Table 1: Experimental space

An environmental chamber and a custom set-up were used for this study, as shown in **Figure 7**. An incandescent light rated for 150W was calibrated using a dimmer switch to deliver exactly 1 sun of irradiance to the devices under testing (DUT). The DUT with a load had a custom holder (**Figure 8**) allowing for the individual cells on a substrate to be connected to a load located outside the chamber. The holder consisted of a laser-cut piece of Teflon with an opening in the center allowing light to penetrate the solar cells. Toothless copper alligator clips were attached to the Teflon piece with aluminum wires, which doubled as leads to the electrical load. The Teflon piece was chosen for its stability over the temperature and humidity ranges of the experiments. The toothless alligator clips were used to make direct contact with the gold anodes and the FTO cathode on the solar cells without damaging them significantly. Maintaining the load outside the chamber at atmospheric conditions ensured that the resistance was not varying over time. The PID controls of the environmental chamber were enabled to maintain constant temperature and humidity, especially when the incandescent light was on. Without them, the temperature in the chamber would overshoot the set value because of the significant heat emanating from the incandescent light.

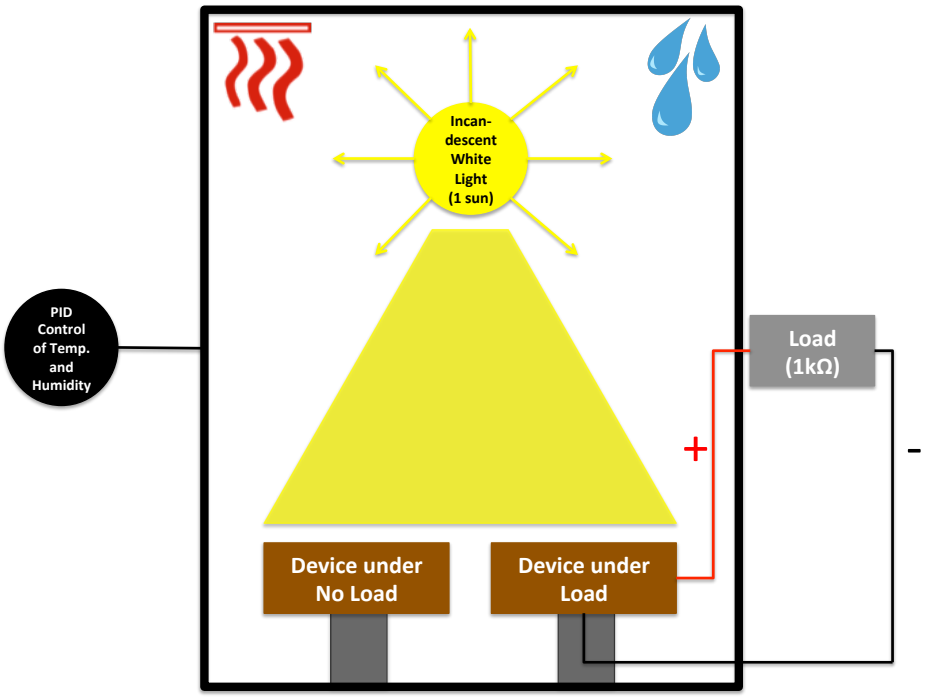

Figure 7: Schematic of the custom degradation set-up installed in the environmental chamber for this study.

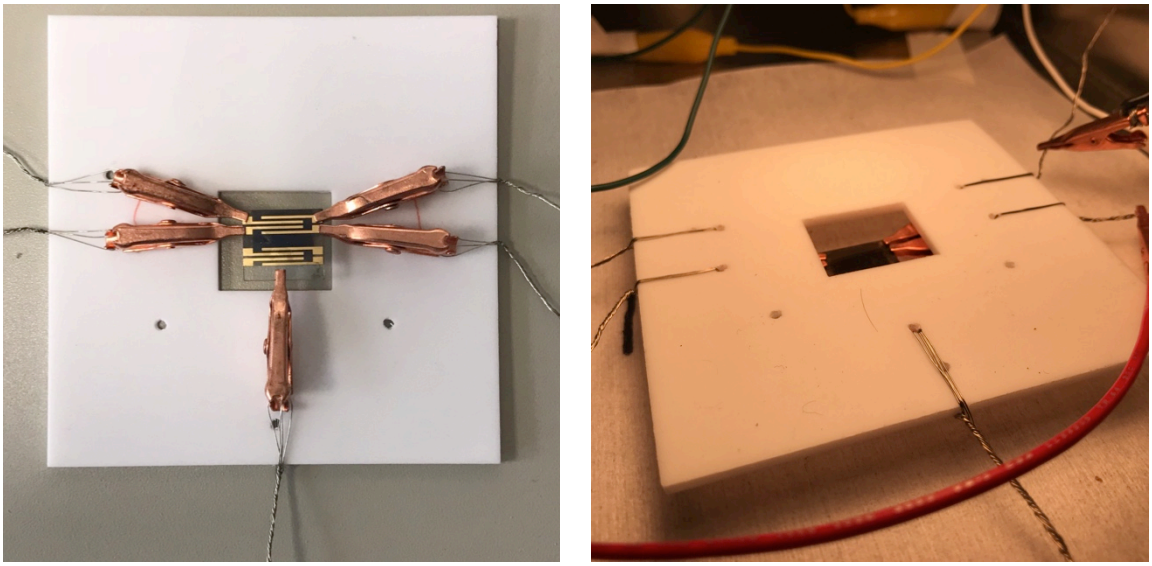

Figure 8: (Left) Top view photograph of the Teflon holder with the toothless alligator clips holding a non-encapsulated solar cell. (Right) Holder + device system under illumination inside the environmental chamber and connected to a load.

The electrical, optical, and crystallographic characteristics of the cells were measured post fabrication and prior to exposure. Then, after cumulative exposure periods of 15, 45, 105, and 225min, those characteristics were again measured to track the degradation. For any given experiment, if the device under testing exhibited 0% efficiency prior to the 225min

cumulative exposure period, the run was cut short. For each experiment a control cell was kept in a N_2 environment and measured at the same periodicity as the devices under testing. The electrical characteristics were measured using a solar simulator delivering an AM1.5 spectrum at 100mW/cm^2 and a Keithley-2400. To ensure the validity of the data collected, the standard solar simulator set-up was improved to limit unnecessary light exposure and speed up the measurements by fully automating the process. Indeed, while performing steady state measurements on cells located on the same substrate, we have noticed that the cells progressively degraded before they were measured, as evidenced in **Figure 9.**

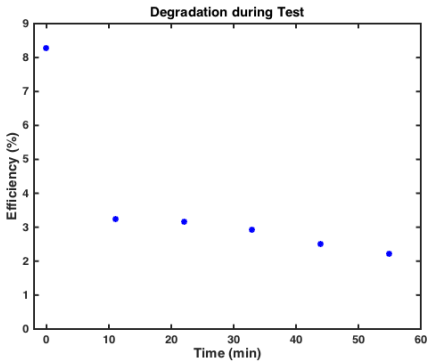

Figure 9: Degradation of the PCE of individual cells on the same substrate during steady state measurements.

To avoid this unwanted behavior outside the environmental chamber, we've made a few improvements to the standard set-up. First, we built a new measurement set-up that connected the data acquisition unit (DAQ) to an Arduino Mega 2560 via a computer. The Arduino microcontroller was in turn connected to low resistance electromagnetic relays, which fed to the devices under testing. To synchronize this circuit, a new MATLAB code was written with a starting block coming from Zimmermann et al. [20]. With this software, we were able to completely measure the devices within 3 min by performing both forward and reverse scans and shutting off the light while the software switched to the next cell to be tested. This system considerably improved the reliability of our measurements.

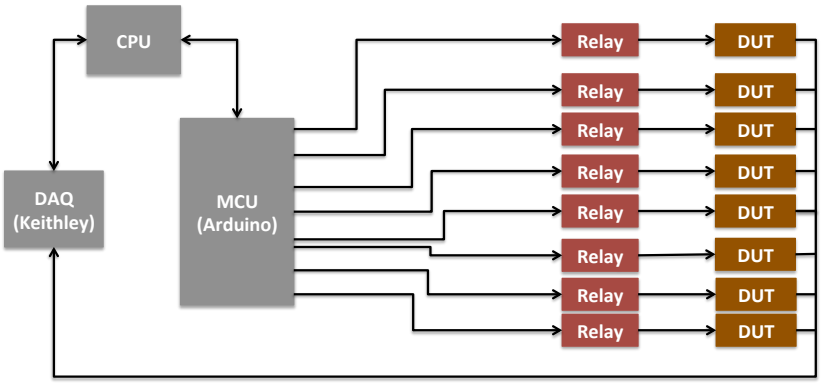

(a)

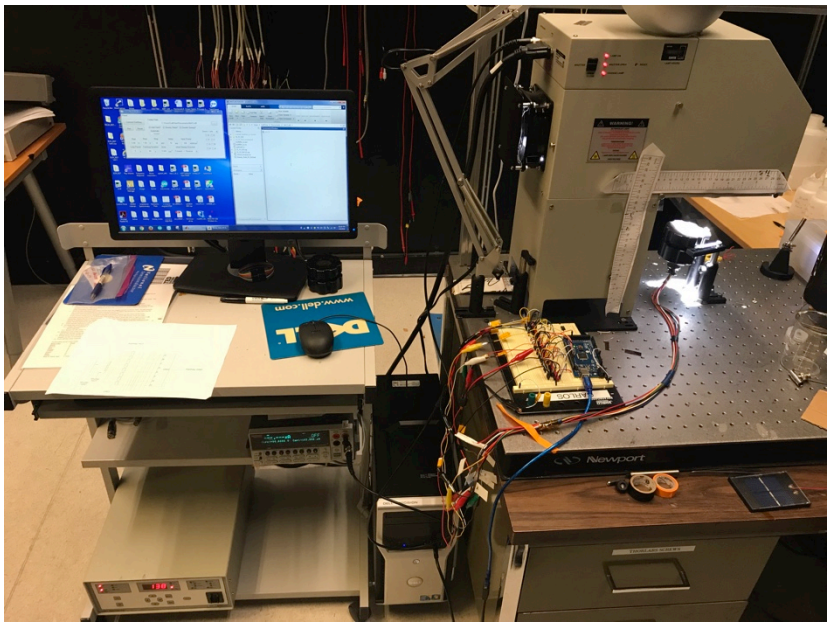

(b)

Figure 10: (a) Schematic representation of the IV measurement set-up. (b) Photograph of its physical implementation.

The JV characteristics were extracted from the forward bias scans, which exhibited slightly lower performance values but were perceived as conservative figures of merit. The absorption spectrum was measured via a UV-Vis spectrometer. Finally, the crystal structure was measured via a coupled angle scan using a Siemens D5000 X-Ray diffractometer. For each XRD spectrum, the final spectrum was obtained by subtracting the spectrum of the FTO/glass substrate from the one of the total stack and applying a digital Savitzky-Golay smoothing filter to make the crystal peaks easier to visualize and identify.

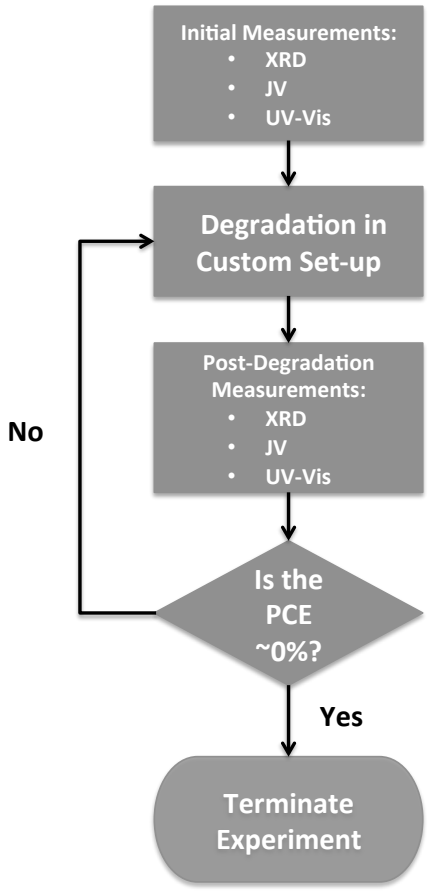

Figure 11: Flow chart summarizing the degradation tracking process for the DUT.

Results and Discussion:

Methodology

The experiments were carried out using the design of experiments (DOE) methodology, which permits the crafting of experiments involving the combination of many competing factors and the subsequent analysis of the responses. As presented in Table 1, we performed 12 out of 16 possible runs, which allows for a partial factorial analysis with 95.4% D-efficiency. The least-squared fit model was employed to reveal the salient factor(s)–with 95% confidence–affecting each responses, which were extracted from three main categories: (1) electrical characteristics represented by the open-circuit voltage (V_{oc}), the short-circuit current density (J_{sc}), the fill factor (FF) and the power conversion efficiency (PCE); (2) optical characteristics represented by the absorption spectra; (3) crystallographic characteristics represented by XRD spectra. To carry out the analysis using the JMP Pro 13 software package, the responses were entered as relative change values between the initial

recorded characteristics of a cell and its measured characteristics by the end of run after 225min of cumulative exposure. Specifically, it meant that the responses were:

- For the electrical characteristics, $\Delta V_{oc} = \frac{V_{225min} - V_{0min}}{V_{0min}}$; $\Delta J_{sc} = \frac{J_{225min} - J_{0min}}{J_{0min}}$;

$$\Delta FF = \frac{FF_{225min} - FF_{0min}}{FF_{0min}};\ \Delta PCE = \frac{PCE_{225min} - PCE_{0min}}{PCE_{0min}}$$

- For the optical characteristics, the integrated absorption spectrum from 300nm to 900nm: $int.abs. = \int_{300nm}^{900nm} abs\ d\lambda\,; \Delta(int.abs.) = \frac{(int.abs.)_{225min} - (int.abs.)_{0min}}{(int.abs.)_{0min}}$
- For the crystallographic characteristics, the full width at half maximum (FWHM) at each salient peak: $\Delta FWHM(2\theta) = \frac{FWHM(2\theta)_{225min} - FWHM(2\theta)_{0min}}{FWHM(2\theta)_{0min}}$

To ensure the statistical significance of the data, the responses were weighed against the controls by subtracting any relative change observed on the control cells from the corresponding relative change observed on the devices under testing (DUT); that is, $\Delta Response = \Delta DUT - \Delta Control$. This methodology ensures that the effects observed are purely due to the conditions of the experiments and not any other uncontrolled background effect.

Effects on the Absorption Spectrum

The analysis reveals that temperature is the only statistically significant factor in the degradation of the absorption of the cells observed. **Figure 12** shows a side-by-side view of a $MAPbI_3$ cell where the only factor changing is the temperature. The cell on the left shows a progressive drop in total absorption located in the 300 to 500nm range of the wavelength spectrum. On the other hand, the cell on the right shows a significant decrease in absorption from 300 nm to the absorption edge at ~770nm, especially after 225min of cumulative exposure period.

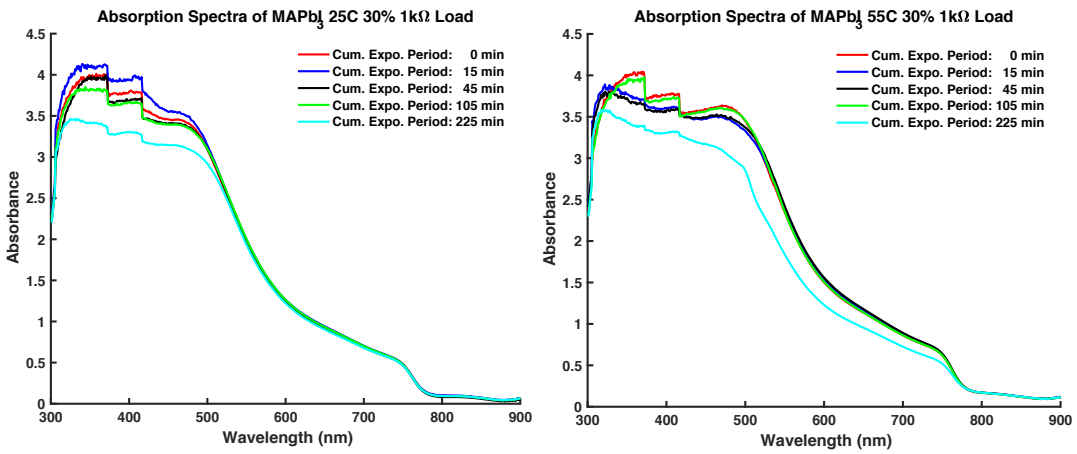

Figure 12: Absorption spectra of $MAPbI_3$ cells degraded for a total cumulative exposure period of 225min at (left) 25°C, 30% humidity, and 1kΩ load, and (right) 55°C, 30 % humidity, and 1kΩ load.

Effects on the Crystal Structure

The XRD spectra reveal up to five prominent crystal peaks at coupled angles of 12.22°, 13.20°, 14.34°/14.54°, 28.50°/28.86°, and 31.90°/32.28°. The peak at 12.22° is present in some samples of the $Cs_{0.2}FA_{0.8}PbI_3$ based devices and appears to be unaffected by any of the degrading factors under study. The peak at 13.20°, characteristic of the presence of PbI_2 appears in degraded samples and is equally affected by the increase in humidity, the type of perovskite used, and the second order interaction between the humidity and the perovskite type, as evidenced in **Figure 13** and **Figure 14**. Indeed, after prolonged exposure at moderate humidity, the $Cs_{0.2}FA_{0.8}PbI_3$ cells appear to dissociate into by-products including PbI_2. The dependence on the interaction between perovskite type and humidity suggests that humidity particularly affects the $Cs_{0.2}FA_{0.8}PbI_3$ in producing PbI_2. The peaks at 14.34° and 14.54° for $Cs_{0.2}FA_{0.8}PbI_3$ and $MAPbI_3$ respectively are also significantly affected by the same factors as the one at 13.20°. At 28.50° for $Cs_{0.2}FA_{0.8}PbI_3$ and 28.86° for $MAPbI_3$, the most significant factors are temperature and the interaction between temperature and perovskite type. Finally, rising temperature is the only significant factor for the FWHM of the peak at 31.90° for $Cs_{0.2}FA_{0.8}PbI_3$, and 32.28° for $MAPbI_3$.

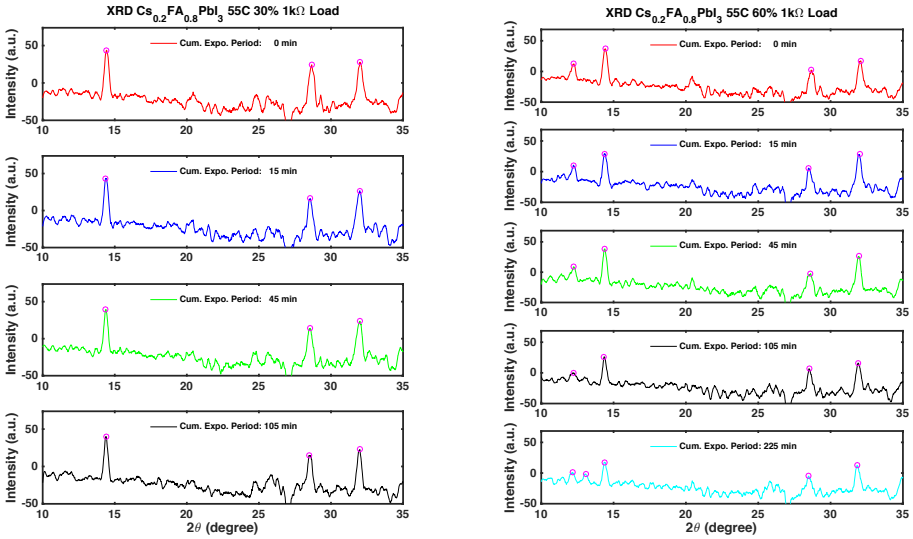

Figure 13: Set of XRD spectra of two $Cs_{0.2}FA_{0.8}PbI_3$ cells undergoing degradation at 55ºC, 30% humidity, and 1kΩ load (left), and 55ºC 60% humidity, and 1kΩ load (right). Notice of the crystal peak at 13.20º on the spectra on the right. The spectra on the left show degradation up to 105min of cumulative exposure period because the efficiency of the cell had already reached 0%.

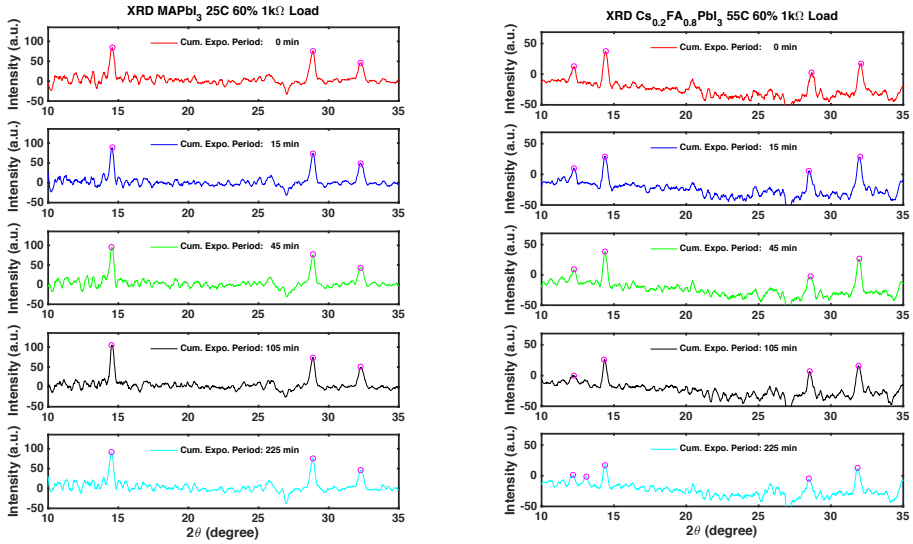

Figure 14: Set of XRD spectra of two perovskite solar cells undergoing degradation. The $MAPbI_3$ is at 25ºC, 60% humidity, and 1kΩ load (left), and the $Cs_{0.2}FA_{0.8}PbI_3$ cell is at 55ºC 60% humidity, and 1kΩ load (right). Notice the absence of peak at 13.20º the $MAPbI_3$ under similar humidity conditions.

Effects on the JV Characteristics

Of the four figures of merit relevant in measuring the electrical characteristics of a solar cell, three showed some dependence on the factors studied: the fill factor, the short-circuit current and the power conversion efficiency. The fill factor has seven dependencies, which are, in order of significance:

1. The humidity,
2. The interaction between the temperature and the perovskite type,
3. The temperature,
4. The interaction between the perovskite type and the humidity,
5. The loading condition,
6. The perovskite type, and
7. The interaction between temperature and the loading condition.

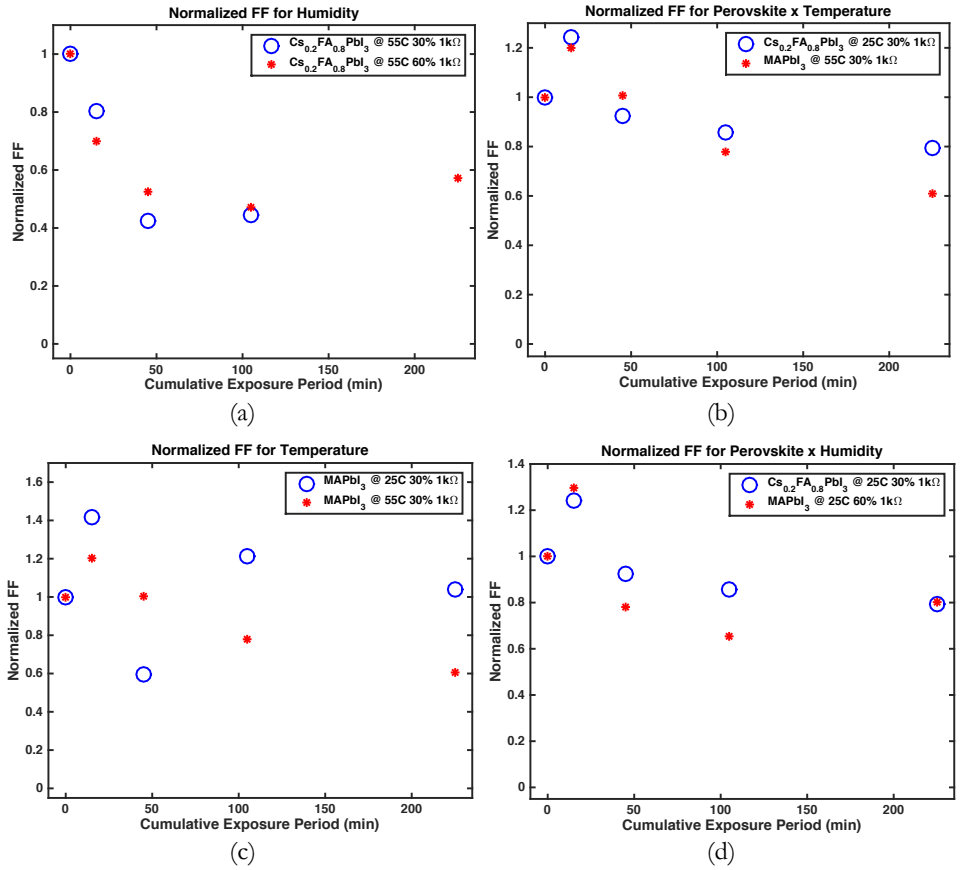

Figure 15: Normalized fill factor for (a) humidity, (b) perovskite type and temperature interaction, (c) temperature, and (d) perovskite type and humidity interaction.

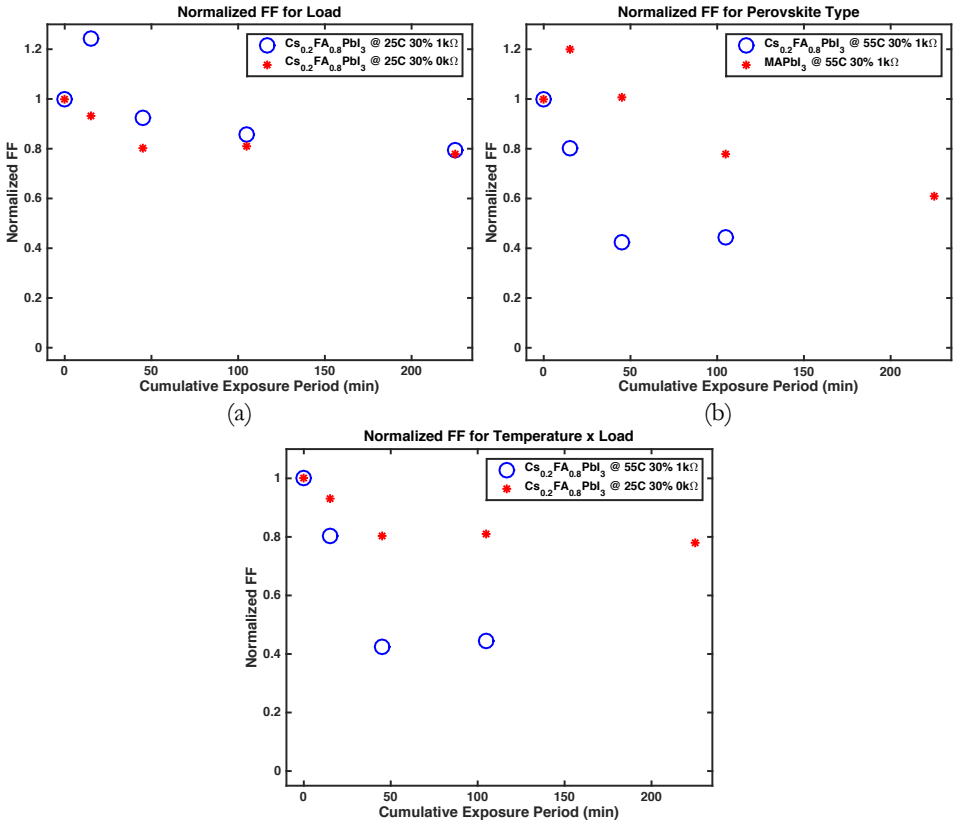

Figure 16: Normalized fill factor for (a) load, (b) perovskite type, and (c) temperature and load interaction.

For the J_{SC}, the perovskite type was the most significant factor exhibiting a higher rate of degradation from $MAPbI_3$ to $Cs_{0.2}FA_{0.8}PbI_3$. The efficiency on the other hand is the only response to significantly depend on three different factors. In order of significance, they are the perovskite type, the temperature, and the humidity.

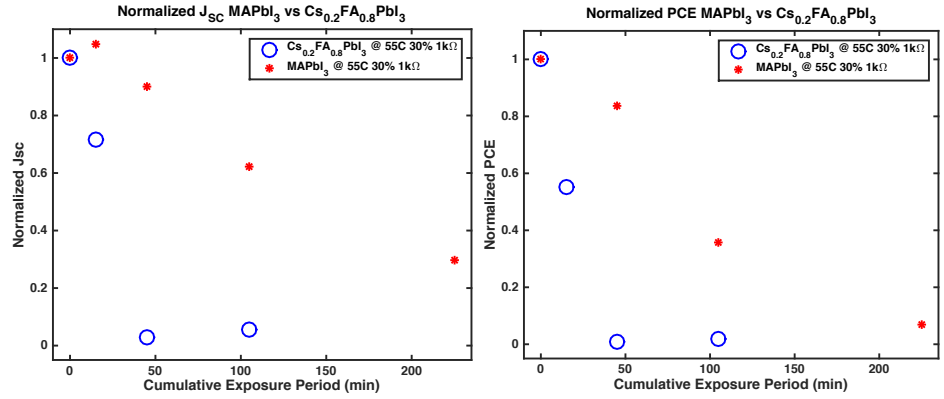

Figure 17: Normalized short-circuit current (left) and power conversion efficiency (right) versus cumulative exposure period for two perovskite types at the same conditions. Notice the higher degradation rate for the $Cs_{0.2}FA_{0.8}PbI_3$ cell.

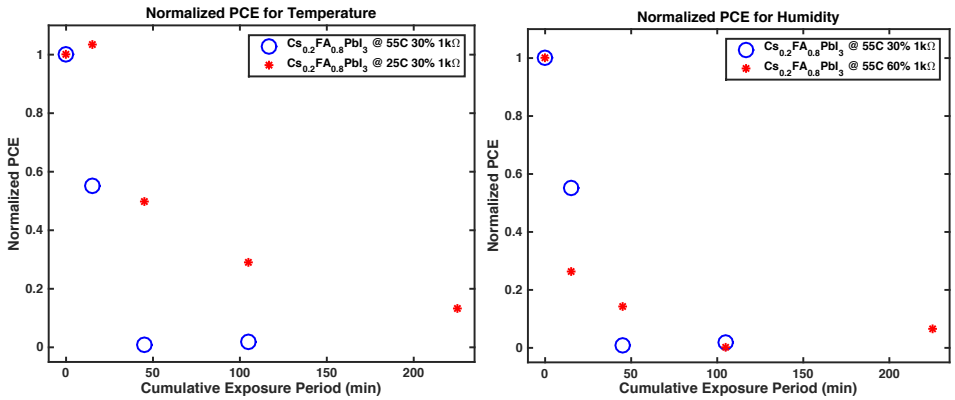

Figure 18: Normalized power conversion efficiency versus cumulative exposure period for temperature (left) and humidity (right).

Interactions between Responses

Employing the DOE method allows us to get a comprehensive view of how responses correlate with one another via a multivariate analysis. The color map in **Figure 19** accompanied by the numerical values of the coefficient of correlation (**Appendix A**) gives a visual representation of this analysis. The open-circuit voltage has a strong dependency on the crystal structure, especially at the 14.34º peak for $Cs_{0.2}FA_{0.8}PbI_3$ and the 14.54º peak for $MAPbI_3$ with a correlation of +0.7691. The other peaks show moderate levels of positive correlation except for the PbI_2 peak at 13.20º that shows a mild negative correlation of -0.2672. For the short-circuit current, outside of the strong correlation with the PCE, which is expected, it has a fair correlation of +0.5662 with the absorption spectrum and a moderately negative correlation of -0.2513 with the crystal peaks at 31.90º ($Cs_{0.2}FA_{0.8}PbI_3$) and 32.28º ($MAPbI_3$). Concerning the fill factor, there is a number of moderate correlations with the other responses. The salient ones are a moderately positive correlation with the absorption, and a moderately negative one with the PbI_2 peak. With regards to the PCE, outside of the strong correlation with the J_{sc}, there are fairly negative correlations with the peaks at 13.20º (-0.4468), and 31.90º ($Cs_{0.2}FA_{0.8}PbI_3$) and 32.28º ($MAPbI_3$) (-0.4410), whereas there are fairly positive correlations with the absorption spectrum and the peak at 12.20º for $Cs_{0.2}FA_{0.8}PbI_3$. Pertaining to the absorption spectrum, the peaks at 13.20º (+0.5065) and 12.22º (-0.4624) show the stronger correlations out of all the other responses. Finally, for the crystallography, the peak at 12.22º has a strong negative correlation with the peak at 13.20º (-0.8108), the peak at 13.20º has a moderately negative correlation of -0.4909 with the ones at 28.50º/28.86º, the peaks at 14.34º/14.54º have fairly strong correlation of +0.6610 with the

ones at 28.50°/28.86°, and the latter have a strong positive correlation of +0.7934 with the peaks at 31.90°/32.28°.

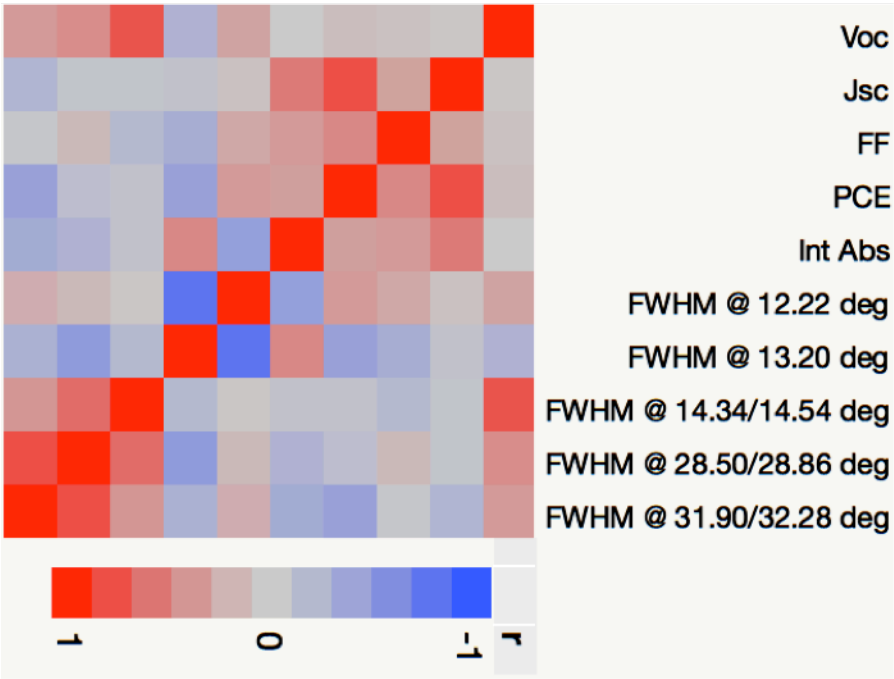

Figure 19: Color map of the coefficients of correlation between the various responses measured

Discussion

There are a few noteworthy observations. First, the fill factor exhibited multiple statistically significant dependencies, including some occurring from interaction factors that would have never been uncovered had we not employed the DOE approach to the design and analysis of these experiments. Furthermore, it shows the complexity in controlling the fill factor and its sensitivity to essentially every possible operating condition. It is however clear that the FF of $Cs_{0.2}FA_{0.8}PbI_3$ cells degrade significantly faster under load at high temperature and humidity levels. This finding supports the underlying purpose of this report in that studying cells in no load situations will not yield in realistic estimates of the degradation. Including the multivariate analysis allows us to hypothesize on the origin of effect as being a combination of current crowding (via the load), reduced photogeneration (reduced absorption), and changes in microstructure with the appearance of PbI_2 coupled with possible strain-stress or fatigue. Further investigation is needed to get a precise answer.

Second, contrary to reports in the literature, the degradation of the lead halide type perovskite solar cells is not necessarily accompanied by the appearance of the lead halide peak. Though we've observed the appearance of the PbI_2 peak from the degradation of a

$Cs_{0.2}FA_{0.8}PbI_3$ cell at 55ºC and 60% humidity, it was the only such case. All the other cells reached their operational limit without any observable appearance of the PbI_2 peak. However, the loss in PCE is accompanied by an increase in FWHM (broader peaks) with increased humidity at some angles, and a decrease in FWHM (sharper peaks) with increased temperature at other angles. These changes in FWHM could be indicative of a few intrinsic processes occurring in the microstructure of the perovskites. It could indicate increased fatigue, an increased strain-stress accumulation, a change in crystal size, and/or an increase in density of point defects in the lattice. Follow up studies will illuminate the underlying mechanism behind this peculiar observation.

Third, the loss in absorption due to temperature increase follows well the loss in short-circuit current and efficiency as a function of temperature as well as the change in crystal structure with temperature. The obvious connection is that the net reduction in absorbed light causes a net loss of photogenerated carriers thus reducing the overall PCE. However, semiconducting materials, like perovskites, usually generate more electron-hole pairs with temperature without generating phonons, especially when they are direct band gap materials. It is possible that one of the processes speculated above could be overshadowing the thermal generation and recombination process.

Fourth, the open-circuit voltage did not show any statistically significant dependence on any single factor studied. However, the V_{oc} is observed to degrade over time, and the multivariate analysis reveals a significant correlation to the changes in crystal structure. Correlation is not causation, and this observation could just be a coincidence given that the controlled factors that resulted in statistically significant dependence for the crystal structure do not show the same relevance for the V_{oc}. Nonetheless, it is possible that the timescale under which the study was undertaken was too short to obtain a definitive result. Another study may be required to answer this conundrum.

Finally, the loss of PCE due to humidity is a process covered ad nauseam in the literature[21], [22]. However, the observations from our experiments show that, under similar conditions, $Cs_{0.2}FA_{0.8}PbI_3$ cells are less stable than the $MAPbI_3$ cells. This is contrary to multiple reports [23], [24] contending that a larger sized A-group in the ABX_3 structure of the perovskite–accomplished via hybridization of the Cs with FA–would result in more stable solar devices. The evidence presented in these reports is quite compelling, so duplicates of these experiments should be run to confirm this observation.

Conclusion:

By controlling four factors (temperature, humidity, perovskite type, and electrical load), the degradation of perovskite solar cells was investigated. A few key observations have arisen as a consequence: (1) the fill factor of $Cs_{0.2}FA_{0.8}PbI_3$ cells degrade significantly faster under load at high temperature and humidity levels; (2) the loss in PCE does not necessarily result in an appearance of a PbI_2 peak in lead halide type perovskites, but could rather be related to other changes in the microstructure; and (3) temperature is a strong degrading element. Further studies are needed to confirm the trends observed and provide a more mechanistic insight onto the stability issues of perovskite solar cells.

Acknowledgements:

This work was made possible by a National Science Foundation Graduate Research Fellowship, a Chancellor's Fellowship, and a Jack Kent Cooke Foundation Graduate Scholarship. Prof. Ana Arias' gracefulness and generosity is applauded for sharing her lab tools, which were critical in carrying out this study to completion. Thanks also go to my collaborators Matthew McPhail and Lance Go for their considerable support. Jeremy Smith, William Scheideler, and Gerd Grau are also hereby recognized for the insightful conversations.

References:

[1] A. Kojima, K. Teshima, Y. Shirai, and T. Miyasaka, "Organometal Halide Perovskites as Visible-Light Sensitizers for Photovoltaic Cells," *J. Am. Chem. Soc.*, vol. 131, no. 17, pp. 6050–6051, May 2009.

[2] M. M. Lee, J. Teuscher, T. Miyasaka, T. N. Murakami, and H. J. Snaith, "Efficient hybrid solar cells based on meso-superstructured organometal halide perovskites.," *Science*, vol. 338, no. 6107, pp. 643–7, Nov. 2012.

[3] NREL, "Best Research-Cell Efficiiencies," 2017. [Online]. Available: https://www.nrel.gov/pv/assets/images/efficiency-chart.png. [Accessed: 04-Jan-2018].

[4] P. A. Basore, "Pilot production of thin-film crystalline silicon on glass modules," in *Conference Record of the Twenty-Ninth IEEE Photovoltaic Specialists Conference, 2002.*, pp. 49–52.

[5] A. Miyata, A. Mitioglu, P. Plochocka, O. Portugall, J. T.-W. Wang, S. D. Stranks, H. J. Snaith, and R. J. Nicholas, "Direct measurement of the exciton binding energy and effective masses for charge carriers in organic–inorganic tri-halide perovskites," *Nat. Phys.*, vol. 11, no. 7, pp. 582–587, Jul. 2015.

[6] W. Li, W. Zhang, S. Van Reenen, R. J. Sutton, J. Fan, A. A. Haghighirad, M. B. Johnston, L. Wang, and H. J. Snaith, "Enhanced UV-light stability of planar heterojunction perovskite solar cells with caesium bromide interface modification," *Energy Environ. Sci.*, vol. 9, no. 2, pp. 490–498, Feb. 2016.

[7] H. C. Weerasinghe, Y. Dkhissi, A. D. Scully, R. A. Caruso, and Y.-B. Cheng, "Encapsulation for improving the lifetime of flexible perovskite solar cells," *Nano Energy*, vol. 18, pp. 118–125, Nov. 2015.

[8] G. Grancini, C. Roldán-Carmona, I. Zimmermann, E. Mosconi, X. Lee, D. Martineau, S. Narbey, F. Oswald, F. De Angelis, M. Graetzel, and M. K. Nazeeruddin, "One-Year stable perovskite solar cells by 2D/3D interface engineering," *Nat. Commun.*, vol. 8, p. 15684, Jun. 2017.

[9] A. J. Pearson, G. E. Eperon, P. E. Hopkinson, S. N. Habisreutinger, J. T.-W. Wang, H. J. Snaith, and N. C. Greenham, "Oxygen Degradation in Mesoporous $Al_2O_3/CH_3NH_3PbI_{3-x}Cl_x$ Perovskite Solar Cells: Kinetics and Mechanisms," *Adv. Energy Mater.*, vol. 6, no. 13, p. 1600014, Jul. 2016.

[10] B. Conings, J. Drijkoningen, N. Gauquelin, A. Babayigit, J. D'Haen, L. D'Olieslaeger, A. Ethirajan, J. Verbeeck, J. Manca, E. Mosconi, F. De Angelis, and H.-G. Boyen, "Intrinsic Thermal Instability of Methylammonium Lead Trihalide Perovskite," *Adv. Energy Mater.*, vol. 5, no. 15, p. 1500477, Aug. 2015.

[11] J. A. Christians, P. A. Miranda Herrera, and P. V. Kamat, "Transformation of the Excited State and Photovoltaic Efficiency of $CH_3NH_3PbI_3$ Perovskite upon Controlled Exposure to Humidified Air," *J. Am. Chem. Soc.*, vol. 137, no. 4, pp. 1530–1538, Feb. 2015.

[12] H. Oga, A. Saeki, Y. Ogomi, S. Hayase, and S. Seki, "Correction to Improved Understanding of the Electronic and Energetic Landscapes of Perovskite Solar Cells: High Local Charge Carrier Mobility, Reduced Recombination, and Extremely Shallow Traps," *J. Am. Chem. Soc.*, vol. 136, no. 48, pp. 16948–16948, Dec. 2014.

[13] H. Oga, A. Saeki, Y. Ogomi, S. Hayase, and S. Seki, "Improved Understanding of the Electronic and Energetic Landscapes of Perovskite Solar Cells: High Local Charge Carrier Mobility, Reduced Recombination, and Extremely Shallow Traps," *J. Am. Chem. Soc.*, vol. 136, no. 39, pp. 13818–13825, Oct. 2014.

[14] E. Edri, S. Kirmayer, A. Henning, S. Mukhopadhyay, K. Gartsman, Y. Rosenwaks, G. Hodes, and D. Cahen, "Why Lead Methylammonium Tri-Iodide Perovskite-Based Solar Cells Require a Mesoporous Electron Transporting Scaffold (but Not Necessarily a Hole Conductor)," *Nano Lett.*, vol. 14, no. 2, pp. 1000–1004, Feb. 2014.

[15] W.-J. Yin, T. Shi, and Y. Yan, "Unusual defect physics in $CH_3NH_3PbI_3$ perovskite solar cell absorber," *Appl. Phys. Lett.*, vol. 104, no. 6, p. 63903, Feb. 2014.

[16] C. Wehrenfennig, G. E. Eperon, M. B. Johnston, H. J. Snaith, and L. M. Herz, "High Charge Carrier Mobilities and Lifetimes in Organolead Trihalide Perovskites," *Adv. Mater.*, vol. 26, no. 10, pp. 1584–1589, Mar. 2014.

[17] J. S. Manser and P. V. Kamat, "Band filling with free charge carriers in organometal halide perovskites," *Nat. Photonics*, vol. 8, no. 9, pp. 737–743, Sep. 2014.

[18] K. Domanski, E. A. Alharbi, A. Hagfeldt, M. Grätzel, and W. Tress, "Systematic investigation of the impact of operation conditions on the degradation behaviour of perovskite solar cells," *Nat. Energy*, pp. 1–7, Jan. 2018.

[19] C. Yi, J. Luo, S. Meloni, A. Boziki, N. Ashari-Astani, C. Grätzel, S. M. Zakeeruddin, U. Röthlisberger, and M. Grätzel, "Entropic stabilization of mixed A-cation ABX_3 metal halide perovskites for high performance perovskite solar cells," *Energy Environ. Sci.*, vol. 9, no. 2, pp. 656–662, Feb. 2016.

[20] E. Zimmermann, K. K. Wong, M. Müller, H. Hu, P. Ehrenreich, M. Kohlstädt, U. Würfel, S. Mastroianni, G. Mathiazhagan, A. Hinsch, T. P. Gujar, M. Thelakkat, T. Pfadler, and L. Schmidt-Mende, "Characterization of perovskite solar cells: Towards a reliable measurement protocol," *APL Mater.*, vol. 4, no. 9, p. 91901, Sep. 2016.

[21] B. Hailegnaw, S. Kirmayer, E. Edri, G. Hodes, and D. Cahen, "Rain on Methylammonium Lead Iodide Based Perovskites: Possible Environmental Effects of Perovskite Solar Cells," *J. Phys. Chem. Lett.*, vol. 6, no. 9, pp. 1543–1547, May 2015.

[22] E. Mosconi, J. M. Azpiroz, and F. De Angelis, "*Ab Initio* Molecular Dynamics Simulations of Methylammonium Lead Iodide Perovskite Degradation by Water," *Chem. Mater.*, vol. 27, no. 13, pp. 4885–4892, Jul. 2015.

[23] J.-W. Lee, D.-H. Kim, H.-S. Kim, S.-W. Seo, S. M. Cho, and N.-G. Park, "Formamidinium and Cesium Hybridization for Photo- and Moisture-Stable Perovskite Solar Cell," *Adv. Energy Mater.*, vol. 5, no. 20, p. 1501310, Oct. 2015.

[24] Z. Li, M. Yang, J.-S. Park, S.-H. Wei, J. J. Berry, and K. Zhu, "Stabilizing Perovskite Structures by Tuning Tolerance Factor: Formation of Formamidinium and Cesium Lead Iodide Solid-State Alloys," *Chem. Mater.*, vol. 28, no. 1, pp. 284–292, Jan. 2016.

Appendix A

	Voc	Jsc	FF	PCE	Int Abs	FWHM @ 12.22 deg	FWHM @ 13.20 deg	FWHM @ 14.34/14.54 deg	FWHM @ 28.50/28.86 deg	FWHM @ 31.90/32.28 deg
Voc	1.0000	0.0460	0.0623	0.1249	0.0192	0.3043	-0.2672	0.7691	0.4727	0.3899
Jsc	0.0460	1.0000	0.3405	0.8095	0.5662	0.0820	-0.0958	-0.0697	-0.0755	-0.2513
FF	0.0623	0.3405	1.0000	0.4844	0.3923	0.3007	-0.3385	-0.2058	0.1426	-0.0437
PCE	0.1249	0.8095	0.4844	1.0000	0.3448	0.3854	-0.4468	-0.0787	-0.1421	-0.4410
Int Abs	0.0192	0.5662	0.3923	0.3448	1.0000	-0.4624	0.5065	-0.0821	-0.2709	-0.3543
FWHM @ 12.22 deg	0.3043	0.0820	0.3007	0.3854	-0.4624	1.0000	-0.8108	0.0446	0.1688	0.2337
FWHM @ 13.20 deg	-0.2672	-0.0958	-0.3385	-0.4468	0.5065	-0.8108	1.0000	-0.2068	-0.4909	-0.3061
FWHM @ 14.34/14.54 deg	0.7691	-0.0697	-0.2058	-0.0787	-0.0821	0.0446	-0.2068	1.0000	0.6610	0.3998
FWHM @ 28.50/28.86 deg	0.4727	-0.0755	0.1426	-0.1421	-0.2709	0.1688	-0.4909	0.6610	1.0000	0.7934
FWHM @ 31.90/32.28 deg	0.3899	-0.2513	-0.0437	-0.4410	-0.3543	0.2337	-0.3061	0.3998	0.7934	1.0000

Table 2: Correlation coefficients used for **Figure 19.** Notice that the color scheme is opposite that of the color map. Dark blue corresponds to strong positive correlation, dark red, strong negative correlation, and gray, little to no correlation.